High-Resolution Peripheral Quantitative Computed Tomographic Imaging of Cortical and Trabecular Bone Microarchitecture in Patients with Type 2 Diabetes Mellitus

Andrew J. Burghardt, Ahi S. Issever, Ann V. Schwartz, Kevin A. Davis, Umesh Masharani, Sharmila Majumdar, and Thomas M. Link

Musculoskeletal Quantitative Imaging Research Group (A.J.B., A.S.I., K.A.D., S.M., T.M.L.), Department of Radiology and Biomedical Imaging, University of California, San Francisco, San Francisco, California 94158; Department of Radiology (A.S.I.), Charité Campus Mitte, Universitaetsmedizin Berlin, 10117 Berlin, Germany; Department of Epidemiology and Biostatistics (A.V.S.), University of California, San Francisco, San Francisco, California 94107; Department of Mechanical Engineering (K.A.D.), University of California, Berkeley, Berkeley, California 94720; and Diabetes Research Center, University of California, San Francisco, San Francisco, California 94143

Context: Cross-sectional epidemiological studies have found that patients with type 2 diabetes mellitus (T2DM) have a higher incidence of certain fragility fractures despite normal or elevated bone mineral density (BMD).

Objective: In this study, high-resolution peripheral quantitative computed tomography was applied to characterize cortical and trabecular microarchitecture and biomechanics in the peripheral skeleton of female patients with T2DM.

Design and Setting: A cross-sectional study was conducted in patients with T2DM recruited from a diabetic outpatient clinic.

Participants: Elderly female patients (age, 62.9 $\pm$ 7.7 yr) with a history of T2DM (n = 19) and age- and height-matched controls (n = 19) were recruited.

Outcome Measures: Subjects were imaged using high-resolution peripheral quantitative computed tomography at the distal radius and tibia. Quantitative measures of volumetric (BMD), cross-sectional geometry, trabecular and cortical microarchitecture were calculated. Additionally, compressive mechanical properties were determined by micro-finite element analysis.

Results: Compared to the controls, the T2DM cohort had 10% higher trabecular volumetric BMD ($P < 0.05$) adjacent to the cortex and higher trabecular thickness in the tibia (13.8%; $P < 0.05$). Cortical porosity differences alone were consistent with impaired bone strength and were significant in the radius (>+50%; $P < 0.05$), whereas pore volume approached significance in the tibia (+118%; $P = 0.1$).

Conclusion: The results of this pilot investigation provide a potential explanation for the inability of standard BMD measures to explain the elevated fracture incidence in patients with T2DM. The findings suggest that T2DM may be associated with impaired resistance to bending loads due to inefficient redistribution of bone mass, characterized by loss of intracortical bone offset by an elevation in trabecular bone density. **(*J Clin Endocrinol Metab* 95: 5045–5055, 2010)**

Abbreviations: aBMD, Areal BMD; ANCOVA, analysis of covariance; BMD, bone mineral density; BMI, body mass index; BV/TV, bone volume/tissue volume; CSA, cross-sectional area; Ct.LF, cortical load fraction; Ct.MOI, cortical MOI; Ct.Po, volumetric index of cortical porosity; Ct.PoV, cortical pore volume; Ct.Th, cortical thickness; CTRL, control; Ct.TMD, cortical tissue mineral density; Ct.vBMD, cortical vBMD; 3D, three-dimensional; DXA, dual x-ray absorptiometry; μFE, micro-finite element; HA, hydroxyapatite; HR-pQCT, high-resolution peripheral QCT; MOI, moment of inertia; mTb.vBMD; medullary Tb.vBMD; pTb.vBMD, peripheral Tb.vBMD; QCT, quantitative computed tomography; Tb.1/N.SD, trabecular number distribution; Tb.N, trabecular number; Tb.Sp, trabecular separation; Tb.Th, trabecular thickness; Tb.vBMD, trabecular vBMD; T2DM, type 2 diabetes mellitus; vBMD, volumetric BMD; VOI, volume of interest.

ISSN Print 0021-972X ISSN Online 1945-7197
Printed in U.S.A.

doi: 10.1210/jc.2010-0226 Received January 28, 2010. Accepted July 23, 2010.
First Published Online August 18, 2010

Type 2 diabetes mellitus (T2DM) is a chronic metabolic disorder associated with impaired glucose metabolism that is often accompanied by a range of systemic complications. A number of cohort studies and recent meta-analyses have found an increased risk of fragility fractures in the humerus, femur, and the distal lower extremity of patients with T2DM (1–8). Schwartz *et al.* (6) found that insulin-treated type 2 diabetics had more than double the risk of foot fractures compared with nondiabetics. These fractures are a serious and well-recognized complication of diabetes mellitus that may significantly impair clinical outcomes for such patients (9). Although factors related to the risk of falling (visual deficits, peripheral neuropathy, *etc.*) may be important discriminants for this population (1), increased bone fragility may also contribute to the elevated risk of fracture. Determination of fracture risk in postmenopausal osteoporosis is primarily based on measures of areal bone mineral density (aBMD) obtained by dual x-ray absorptiometry (DXA). However, cross-sectional epidemiological studies have generally found that, despite the elevated incidence of certain types of fragility fractures, type 2 diabetics generally have equivalent (10–12) or even higher (2, 13–18) aBMD compared with matched controls (CTRLs). Therefore, bone mineral density (BMD) is of limited utility for assessing fracture risk in this patient population, and new investigational methods for exploring fracture etiology related to diabetes mellitus are critically needed. Specifically, there is a need to measure bone quality factors related to bone strength that are not captured by projectional x-ray techniques. These include volumetric density, cross-sectional geometry, cortical and trabecular microarchitecture, and tissue composition. In this context, high-resolution quantitative three-dimensional (3D) imaging techniques are particularly well suited as a clinical research tool to investigate bone quality in patients with T2DM.

High-resolution peripheral quantitative computed tomography (HR-pQCT) has recently been introduced as a noninvasive method for *in vivo* 3D characterization of bone in the peripheral skeleton (distal radius and tibia). Similar to traditional quantitative computed tomography (QCT), HR-pQCT provides the ability to quantitatively assess volumetric BMD (vBMD) independently in cortical and trabecular compartments. Additionally, due to the high isotropic nominal resolution of this modality (82 μm), the ability to quantify geometric, microarchitectural, and mechanical features of cortical and trabecular bone has also been established (19–21). This imaging technique has been applied in a number of cross-sectional studies to characterize aging effects (22–27), fracture discrimination (28–31), and various pathologies (32–34) frequently, but not exclusively, in the context of postmenopausal bone loss in women.

In this pilot study, HR-pQCT was applied to image the peripheral skeleton of postmenopausal women with T2DM. This population was selected because the increase in nonvertebral fracture risk associated with T2DM has been more definitively established compared with men (35). T2DM-related changes in bone quality, coincident with estrogen-deficient bone loss, may compound fracture risk, and therefore this is a particularly important population to characterize. Our hypothesis was that type 2 diabetics have unique structural deficiencies that result in compromised bone strength, compared with CTRLs without diabetes. This would suggest that the discrepancy between fracture incidence and DXA findings in the T2DM epidemiological literature can be attributed, in part, to differences in bone quality not detected by aBMD. To that end, we calculated measures of density, cross-sectional geometry, trabecular microarchitecture, cortical porosity, and compressive biomechanics from the HR-pQCT image data acquired for our T2DM cohort and an age-, height-, and ethnicity-matched CTRL cohort.

Subjects and Methods

Subjects

For this cross-sectional study, postmenopausal female patients with T2DM (n = 19) were recruited from a local diabetic outpatient clinic by a coinvestigator of the study (U.M.). Inclusion criteria required patients to have a history of diabetes for a minimum of 5 yr and a body mass index (BMI) between 19 and 35 kg/m^2, to be fully ambulatory at the time of the exam, and to not have a recent history of long periods of inactivity. In accordance with the American Diabetes Association criteria, diabetes was defined as self-report of diabetes previously diagnosed by a physician, use of hypoglycemic medications, or a fasting glucose greater than 126 mg/dl (7.0 mM). Age, ethnicity, and height-matched CTRLs were recruited through public media and posted flyers. Additionally, eight subjects matching the inclusion/exclusion criteria were cross-enrolled from a normative cross-sectional study (36) to equalize the number of subjects in the CTRL group (n = 19 total). Exclusion criteria were as follows: history of severe neuropathic disease, alcoholism, chronic drug use, chronic gastrointestinal disease, renal or hepatic impairment, unstable cardiovascular disease, high-energy trauma, and pathological skeletal fractures. Patients with a history of treatment with the following medications were also excluded: rosiglitazone, pioglitazone, adrenal or anabolic steroids, anticonvulsants, anticoagulants, fluoride, bisphosphonates, calcitonin, or tamoxifen. The University of California, San Francisco Committee of Human Research approved the study protocol, and all patients gave written, informed consent before participation.

HR-pQCT imaging

All subjects were imaged in a clinical HR-pQCT system (XtremeCT; Medical AG, Brüttisellen, Switzerland) using a stan-

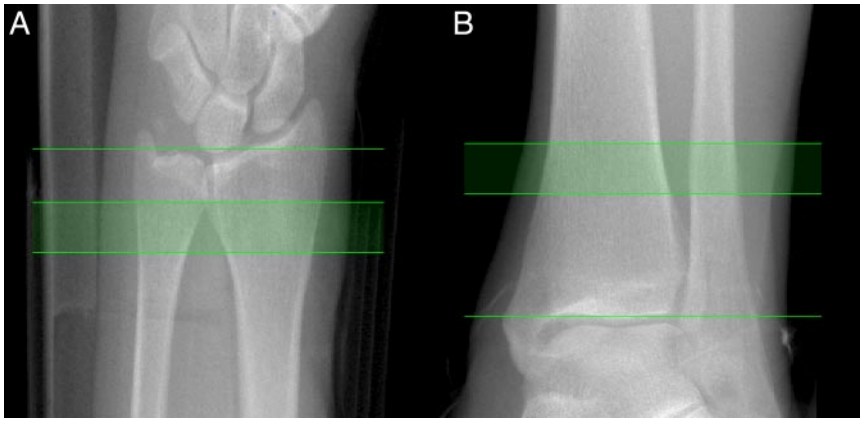

FIG. 1. Representative scout radiographs for the radius (A) and tibia (B) illustrating the localization for the tomographic acquisition (*filled green*).

dard *in vivo* protocol described in previous patient studies (15–17). The subject's nondominant forearm and leg were immobilized in a carbon fiber cast that was fixed within the gantry of the scanner. If the subject reported a previous extremity fracture at that site, the contralateral forearm or leg was examined. A single dorsal-palmar projection image of the distal radius/tibia was acquired to define the tomographic scan region (Fig. 1, A and B). This region spanned 9.02 mm in length (110 slices) and was fixed starting at 9.5 mm and 22.5 mm (for the radius and tibia, respectively) proximal from the mid-jointline, and extending proximally. For tomography, 750 projections were acquired over 180° with a 100-msec integration time at each angular position. The 12.6-cm field of view was reconstructed across a 1536 × 1536 matrix using a modified Feldkamp algorithm, yielding 82-μm voxels (37). Total scan time was 2.8 min, with an effective dose of approximately 4.2 μSv for each site, comparable to the dose received from a standard chest x-ray or DXA procedure. The images were calibrated to hydroxyapatite (HA) concentration based on a separate measurement of a phantom comprised of several rods with a range of mixtures of HA and a soft tissue equivalent organic resin. This calibration procedure is based on the methods originally established for desktop microtomography (38).

Image analysis

HR-pQCT images were evaluated using the standard clinical evaluation protocol, adapted from methods developed for a previous peripheral QCT device (39, 40). Trabecular bone volume fraction [bone volume/tissue volume (BV/TV)] was derived from the vBMD of the trabecular compartment (Tb.vBMD) using the assumption that compact bone has a matrix mineral density of 1200 mg HA/cm^3, whereas the marrow background is equivalent to 0 mg HA/cm^3. Tb.vBMD was also calculated for two concentric subregions: a peripheral region adjacent to the cortex (pTb.vBMD) and a central medullary region (mTb.vBMD) (Fig. 2, A and B). The peripheral region was defined such that it extended from the endosteal boundary centrally, covering 40% of the cross-sectional area (CSA). In addition to vBMD measures, aBMD was calculated for the distal radius from the HR-pQCT images using an automated approach (41). The trabecular structure was extracted using a Laplace-Hamming filter—which effectively smoothes the image and enhances edges—followed by a fixed global threshold (42). From the binary image, trabecular number (Tb.N) and its distribution (Tb.1/N.SD) were measured using direct 3D methods (43, 44). Based on the densitometric BV/TV and direct Tb.N, trabecular thickness (Tb.Th) and trabecular separation (Tb.Sp) were derived using traditional plate model assumptions. The reproducibility of density-based measures is generally less than 1% and typically between 3 and 5% for bone structure parameters (22, 45–47).

As reported previously, the default cortical bone analysis provided with this HR-pQCT device performs poorly for subjects with thin or porous cortices (45, 48). Accordingly, a fully automated cortical compartment segmentation technique adapted from the method described originally by Buie *et al.* (48, 49) was applied. Based on this segmentation, cortical vBMD (Ct.vBMD) and cortical tissue mineral density (Ct.TMD) were calculated. Ct.vBMD was simply the mean mineralization of all voxels in the cortical volume of interest (VOI), whereas Ct.TMD was calculated as the mean of only mineralized voxels in the cortical VOI (*i.e.* based on the same segmentation of mineralized voxels used for the trabecular structure analysis). Additionally, for Ct.TMD, partial volume contributions were suppressed by peeling two voxels from all surfaces. The average maximal second moment of inertia (MOI) for the cortex (Ct.MOI) and total cross-section were calculated from the segmented binary images to provide an estimate of bending strength. A volumetric index of cortical porosity, denoted Ct.Po, was calculated as previously described by Burghardt *et al.* (36, 50) based on the cortical pore volume (Ct.PoV) and the mineralized cortical bone volume (Ct.BV):

$$Ct.Po = \frac{Ct.PoV}{Ct.PoV + Ct.BV}$$

Based on this segmentation, a direct 3D calculation (43) of cortical thickness (Ct.Th) was performed on the composite segmentations of the mineralized cortex and porosity, thereby dis-

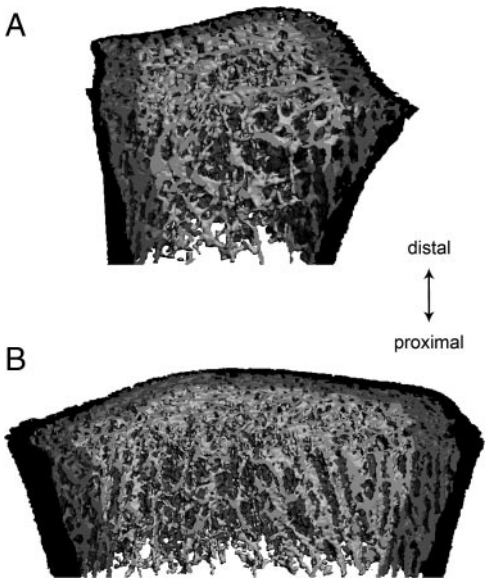

FIG. 2. Two-dimensional illustration of the segmented compartments included in the quantitative image analysis of the radius (A) and tibia (B): cortical bone (*black*), peripheral trabecular bone (*dark gray*), and medullary trabecular bone (*light gray*).

TABLE 1. Least significant change and root-mean-square coefficient of variation of quantitative cortical bone measures

Parameter	Radius	Tibia
Ct.vBMD (mg HA/cm^3)	17 (0.8%)	14 (0.6%)
Ct.TMD (mg HA/cm^3)	10 (0.4%)	9 (0.3%)
Total area (mm^2)	0.8 (0.1%)	1.1 (0.1%)
Cortical area (mm^2)	1.9 (1.5%)	5.0 (1.7%)
Trabecular area (mm^2)	2.0 (0.4%)	5.0 (0.4%)
Ct.Th (mm)	0.08 (3.9%)	0.05 (1.5%)
Ct.PoV (mm^3)	2.19 (12.0%)	10.4 (5.3%)
Ct.Po (%)	0.57 (11.7%)	0.92 (3.9%)

regarding intracortical pore surfaces in the local distance calculations. This index represents a direct, 3D measure of endosteal-periosteal distance. The least significant change and root-mean-square coefficient of variation for these parameters are described in Table 1 from reproducibility measurements in 27 postmenopausal women (50).

Micro-finite element (μFE) analysis

Linear micro-finite element (μFE) analysis was applied to calculate apparent biomechanical properties under uniaxial compression. Homogeneous mechanical properties were assumed for all bone elements. The binary image data set was converted to a mesh of isotropic brick elements using a voxel conversion technique (51), and each element was assigned an elastic modulus of 10 GPa (52) and a Poisson's ratio of 0.3 (53). Cortical and trabecular bone elements were labeled as different materials, with identical material properties to facilitate calculation of compartmental load distribution. A uniaxial compression test in the axial direction (superior-inferior) was performed with an applied strain of 1%. An iterative solver (Scanco FE Software v1.12; Scanco Medical AG) was used to compute reaction forces at the proximal and distal ends of the scan region for the prescribed displacements. For each model, stiffness (K), apparent modulus (E), and the load fraction for the cortical compartment (Ct.LF) at the distal boundary were calculated. Furthermore, failure load (F) was estimated using methods previously described by Pistoia *et al.* (54). Differential biomechanical indices related to Ct.Po were also calculated by running a second model for each specimen with the intracortical pore spaces digitally occluded (36). Specifically, the deficit in stiffness (ΔK), apparent modulus (ΔE), and failure load (ΔF) due to the resolvable Ct.Po were calculated as the difference in the respective parameter between the occluded and original models, and normalized by the original. These indices were reported as a percentage. The fractional load (ΔCt.LF) shifted from the cortex to the trabecular bone was calculated simply as the difference between occluded and original Ct.LF.

Statistical analysis

Mean and SD were calculated for all indices and were determined for each site (radius and tibia) and study group (CTRL and T2DM). Because the Shapiro-Wilk W test revealed that multiple parameters were not normally distributed, group-wise differences were evaluated for statistically significant differences using the Wilcoxon rank sum test with $\alpha = 0.05$. Because the mean weight of the T2DM group was statistically greater than the CTRL group ($P < 0.05$), analysis of covariance (ANCOVA) was additionally applied to test for statistical significance after correcting for weight as a covariate. The interaction between weight and T2DM status was tested for each measure, and because the slopes were not statistically different between T2DM and CTRL, the ANCOVA was performed assuming covariate homogeneity between groups (*i.e.* equal slopes).

TABLE 2. Descriptive data of study participants

	CTRL	T2DM	*t* test
n	19	19	
Age (yr)	62.6 ± 6.8	62.9 ± 7.7	ns
Height (cm)	158.4 ± 6.7	160.2 ± 6.9	ns
Weight (kg)	67.4 ± 11.5	78.2 ± 18.2	$P < 0.05$
BMI (kg/m^2)	26.8 ± 3.5	30.1 ± 5.4	$P < 0.05$
No. of fractures	0	2	

ns, Not significant.

Results

Subjects

A summary of the characteristics of patients recruited for this study is presented in Table 2. The CTRL group was comprised of six Caucasian, one African-American, six Hispanic, and six Asian subjects, whereas the T2DM group was comprised of six Caucasian, five African-American, four Hispanic, and four Asian subjects. As expected, given height and age matching, the T2DM cohort had a higher average body mass and BMI compared with the CTRL group ($P < 0.05$). As a result, statistical correction for weight was performed in addition to standard ANOVA for T2DM and CTRL comparisons. Because ANCOVA did not significantly change the results, the uncorrected results (Wilcoxon rank sum test) are reported in detail, and corrected differences are noted where appropriate. Of the 19 patients with T2DM, two had previous fractures. One patient had a history of fracture at the femoral head and ankle. The second patient had a previous proximal humerus fracture and a grade II fracture of the L5 vertebrae, as determined from radiographic analysis using the semiquantitative method of Genant *et al.* (55).

HR-pQCT imaging

Representative HR-pQCT images of the distal radius and tibia for the median (by vBMD) CTRL, T2DM, and T2DM with fracture subjects are shown in Figs. 3 and 4. The fracture subjects in particular showed dramatic levels of intracortical porosity in the distal radius and tibia as well as extremely dense trabecular bone in the peripheral region adjacent to the cortex. Additionally, the presence of severe arterial calcifications in the soft tissue surrounding the bone was observed in five T2DM subjects (26%), including both fracture subjects (Fig. 5). Arterial calcifications were not observed in the CTRL group.

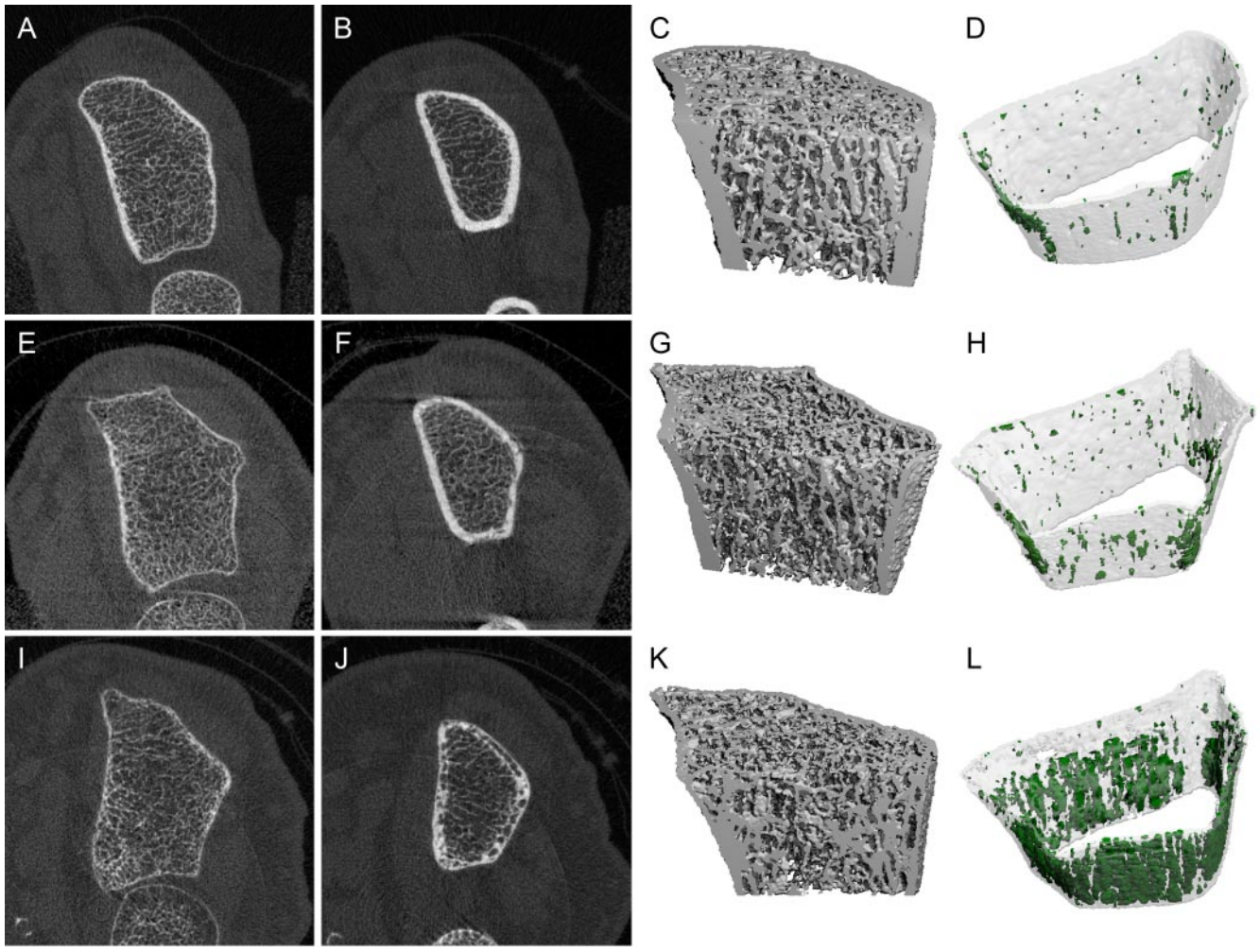

FIG. 3. Median (by total vBMD) HR-pQCT images of the distal radius from CTRL (*top*), T2DM (*middle*), and T2DM with fracture (*bottom*): distal-most slices (A, E, I); proximal-most slices (B, F, J); 3D visualization of the mineralized bone structure (C, G, K); and 3D visualization of cortical bone (*transparent gray*) and Ct.Po. (*solid green*) (D, H, L).

Image analysis

Of the 38 total datasets, the automated cortical bone compartment segmentation was qualitatively acceptable for all but the two fracture subjects. In these subjects, extensive Ct.Po and endocortical trabecularization was evident and led to poor detection of the endocortical boundary. As a result, manual adjustments to the endocortical contour were required for both the radius and tibia scans of these subjects. The mean and SD for all density, cross-sectional geometry, microarchitectural, and biomechanical indices are reported in Table 3. The percentage difference between T2DM and CTRL groups is also reported, with statistically significant differences indicated where appropriate.

At both sites, the majority of bone quality markers were found to be consistent with equivalent or greater estimates of bone strength for the T2DM cohort compared with CTRL. aBMD of the distal radius was effectively the same between groups. In the distal tibia, vBMD was significantly higher ($P < 0.05$) in the T2DM group. This was primarily due to a 10% greater trabecular density ($P < 0.05$) in the peripheral region adjacent to the cortex (pTb.vBMD).

Minor differences in cross-sectional geometry were observed and were generally muted when corrected for weight. After statistical correction for weight, total and cortical maximal MOI tended to be lower for the T2DM cohort, although these trends did not reach statistical significance. In the distal tibia, Tb.Th was significantly higher in the T2DM group (+13.8%; $P < 0.05$). Estimates of bone strength determined by μFE modeling of an axial compressive load tended to be higher for T2DM subjects, with apparent modulus reaching statistical significance (+10.6%; $P < 0.05$).

The only measures indicating compromised bone quality were related to Ct.Po, where Ct.PoV and Ct.Po were 151 and 124% higher, respectively, in the radius of the T2DM cohort. In the tibia, the trends were similar (118 and 36%, respectively) but were shy of statistical significance. Porosity in the distal radius of these subjects

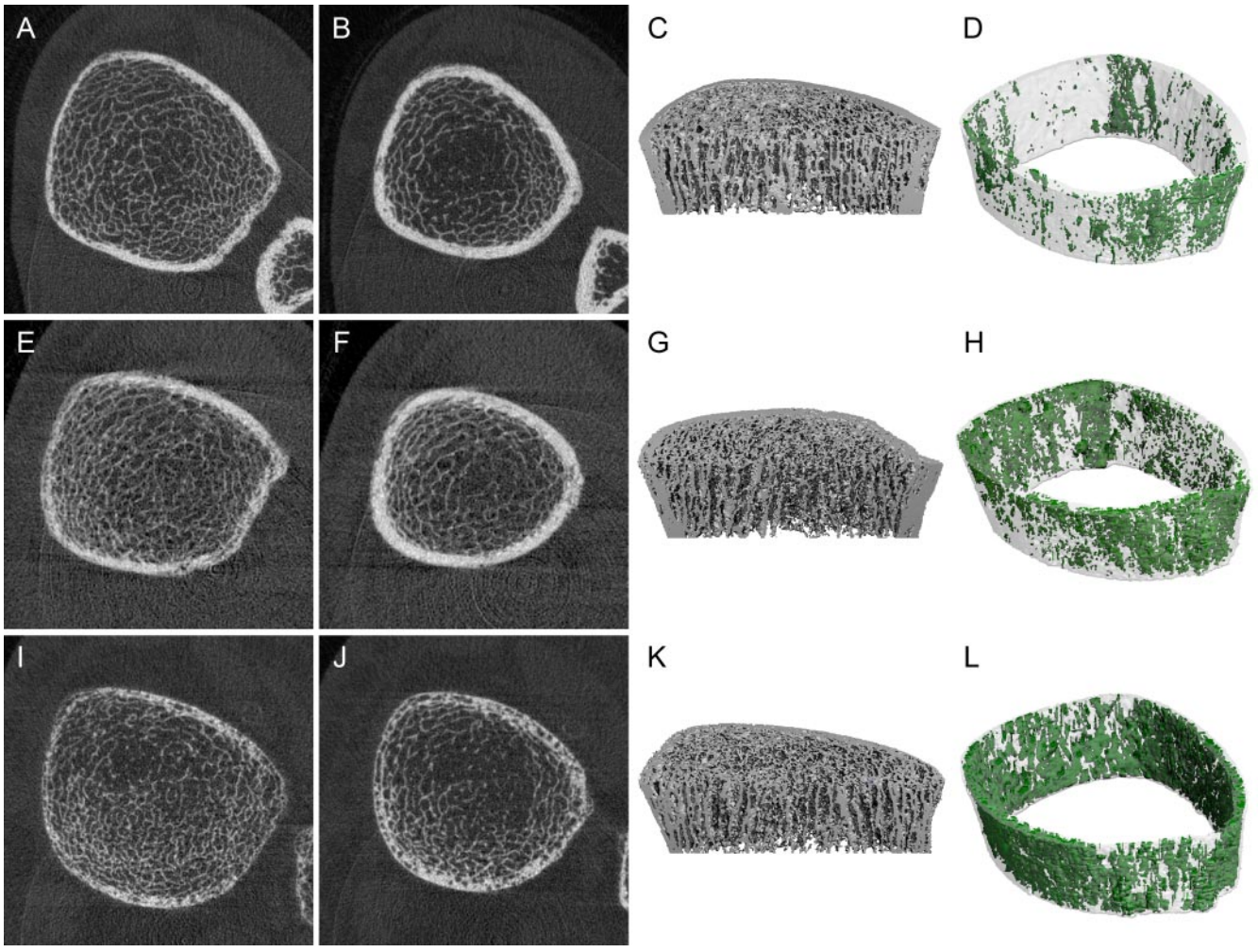

FIG. 4. Median (by total vBMD) HR-pQCT images of the distal tibia from CTRL (*top*), T2DM (*middle*), and T2DM with fracture (*bottom*): distal-most slices (A, E, I); proximal-most slices (B, F, J); 3D visualization of the mineralized bone structure (C, G, K); and 3D visualization of cortical bone (*transparent gray*) and Ct.Po (*solid green*) (D, H, L).

was specifically associated with a 2.5–3.0% deficit in compressive biomechanical properties, compared with a 1.7–1.9% deficit in the CTRL cohort ($P < 0.05$). After statistical correction for weight, the group-wise differences generally decreased, although the relative effects exhibited similar trends to the uncorrected differences.

Discussion

A number of cross-sectional studies have documented the increased fracture incidence of individuals with T2DM (1–8) despite equivalent or higher aBMD measures compared with matched CTRLs (2, 10–18). This is often attributed to a greater risk for falls due to visual deficiencies, peripheral neuropathy, and other complications commonly associated with T2DM (1). Another possible explanation for this discrepancy is that bone quality factors not captured by two-dimensional projectional densitometry may compromise bone strength in this population. In this pilot investigation, we have used HR-pQCT to characterize 3D bone density, geometry, microarchitecture, and compressive biomechanics in a limited cohort of postmenopausal female patients with T2DM and compared with age- and height-matched CTRLs.

In general, the density, geometric, microarchitectural, and biomechanical differences between the T2DM and CTRL cohorts were consistent with comparable or even greater bone quality and compressive strength in the T2DM cohort. When statistically corrected for body mass, these differences were generally more muted. The observed trend toward higher Tb.vBMD in T2DM subjects is in agreement with other recent imaging studies based on lower resolution modalities (14, 56). Ct.Po-related measures alone were significant indicators of compromised bone quality. This is an important observation because the cortical ultra- and microarchitecture are important determinants of bone strength (57), and specifically, are critical to fracture initiation and propagation under bending

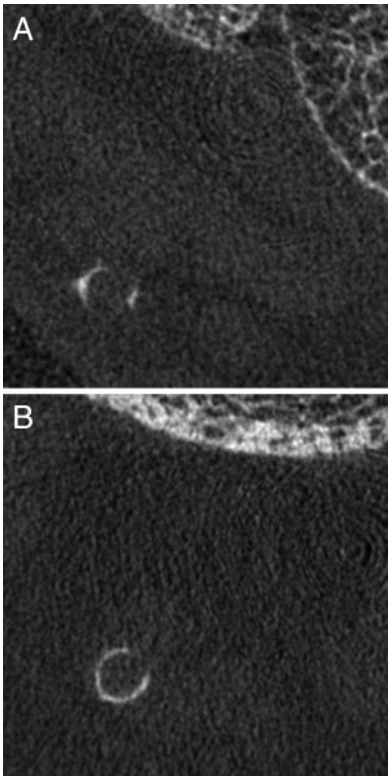

FIG. 5. HR-pQCT images illustrating arterial calcifications in the distal radius (A) and distal tibia (B) of a subject with T2DM and a history of lower extremity fragility fracture.

loads (58). Although it is not possible to realistically simulate bending loads from HR-pQCT scans that span only 1 cm along the length of the bone, the cross-sectional MOI parameters were reported as surrogates for bending strength. After correction for body mass, total and cortical maximal MOI tended to be lower in T2DM subjects relative to CTRL. Although these differences failed to reach statistical significance in our limited cohort (n = 19 per group), they are consistent with a deleterious effect on bending strength.

The dense trabecular bone in the peripheral cancellous compartment and elevated pTb.vBMD of T2DM patients did not visually appear to be due to endocortical trabecularization artifactually included in the cancellous VOI. Despite significant intracortical erosion in these subjects, the extant endocortical boundary is still visually discernable (Fig. 4). The manual adjustments made to the automated endocortical contour generated during the segmentation process ensured that these features were appropriately assigned to the trabecular compartment. Instead, this hyperdense structure is likely the result of trabecular thickening in this region, possibly a compensatory adaptation for the loss of bone mass in the cortex. This adaptation would be particularly necessary in a habitually loaded skeletal site such as the tibia to provide sufficient compressive rigidity to support the greater weight of a diabetic individual, but it would be less efficient with respect to bending loads.

In a subcohort of the Osteoporotic Fractures in Men (MrOS) study using pQCT, Petit *et al.* (56) reported that men with T2DM had cortical bone geometry deficits despite higher aBMD compared with CTRLs. Whereas they found smaller CSA in T2DM men compared with CTRLs (significant after correction for weight), the results of this study indicated a trend toward greater CSA for a female T2DM cohort (not statistically significant). They proposed that the smaller CSA is a possible explanation for the observed elevated aBMD, compared with matched CTRLs. In a small cross-sectional QCT study that included men and women with T2DM, Melton *et al.* (14) observed differences related to diabetes within each gender cohort consistent with the results of both MrOS and the present study. Several studies in small animal models of hyperglycemic T2DM have found reduced cross-sectional geometric properties and compromised bending strength compared with control animals (59–61). However, it is difficult to draw direct comparisons with respect to cortical structure because rodents lack the intracortical Haversian remodeling surfaces that give rise to the porosity observed in this study in humans.

The use of a high-resolution *in vivo* clinical imaging device with a spatial resolution at the trabecular level was a particular strength of this study. This advantage allowed a more detailed evaluation of both trabecular and cortical microarchitecture not previously possible with lower-resolution *in vivo* modalities (14, 56). Specifically, increased Ct.Po was identified as a possible explanation for the increased peripheral fracture incidence for T2DM women, compared with matched CTRLs, despite favorable aBMD scores. The μFE results support the deleterious biomechanical impact of Ct.Po in this cohort; whereas absolute estimates of compressive bone strength were equivalent or even greater than CTRL, porosity-specific biomechanical deficits were significantly higher in the T2DM cohort and offset by higher Tb.vBMD.

Notably, the porosity-related parameters have substantially greater variability compared with CTRL. In part, this can be attributed to the contribution of the two fracture subjects that were found to have Ct.Po 2-fold greater than the mean for the T2DM group. Nevertheless, when these subjects were excluded from the statistical analysis, the variability of the T2DM group remained somewhat greater than CTRL. Additionally, whereas excluding the fracture subjects reduced the porosity-related differences between T2DM and CTRL, the trends for higher porosity and associated biomechanical deficits generally remained significant or approaching significance. The greater variability

TABLE 3. Density, cross-sectional geometry, microarchitectural, and biomechanical parameters for controls and T2DM patients

Parameter	Radius			Tibia		
	CTRL	T2DM	%Δ	CTRL	T2DM	%Δ
Density						
aBMD (g/cm^2)	0.32 ± 0.06	0.33 ± 0.06	3.7%			
vBMD (mg HA/cm^3)	297 ± 68	291 ± 49	−2.2%	269 ± 45	293 ± 45	**9.2%**[a]
Tb.vBMD (mg HA/cm^3)	142 ± 41	144 ± 25	1.2%	140 ± 34	159 ± 34	13.1%
pTb.vBMD (mg HA/cm^3)	200 ± 42	206 ± 27	2.9%	206 ± 36	227 ± 33	**10.0%**[a]
mTb.vBMD (mg HA/cm^3)	102 ± 42	101 ± 26	−1.1%	95 ± 34	112 ± 37	17.8%
Cross-sectional geometry						
Total area (mm^2)	245 ± 42	257 ± 43	5.1%	642 ± 108	649 ± 120	1.0%
Cortical area (mm^2)	47.2 ± 12	47.3 ± 13	0.3%	108 ± 24	116 ± 28	7.8%
Trabecular area (mm^2)	192 ± 42	203 ± 40	5.7%	529 ± 107	524 ± 109	−0.8%
MOI (mm^4)	1,794 ± 559	2,088 ± 709	16.3%	15,029 ± 4,826	16,583 ± 6,444	10.3%
Ct.MOI (mm^4)	1,191 ± 340	1,374 ± 441	15.4%	8,578 ± 2,738	9,765 ± 3,157	13.8%
Microarchitecture						
Tb.N (mm^{-1})	1.77 ± 0.32	1.84 ± 0.30	3.4%	1.75 ± 0.41	1.73 ± 0.39	−0.9%
Tb.Th (μm)	66.0 ± 10.4	65.4 ± 7.4	−0.9%	67.8 ± 13.3	77.2 ± 12.7	**13.8%**[a]
Tb.Sp (μm)	513 ± 100	492 ± 91	−4.0%	534 ± 136	532 ± 160	−0.5%
Tb.1/N.SD (μm)	248 ± 94	213 ± 55	−14.4%	258 ± 82	253 ± 92	−2.0%
Biomechanics						
Stiffness, *K* (kN/mm)	64 ± 14	66 ± 13	2.6%	172 ± 33	194 ± 39	12.5%
Modulus, *E* (MPa)	1,751 ± 433	1,708 ± 270	−2.5%	2,158 ± 417	2,388 ± 343	**10.6%**[a]
Failure load, *F* (n)	3,246 ± 680	3,340 ± 645	2.9%	8,757 ± 1,707	9,734 ± 1,956	11.2%
Ct.LF (%)	51.6 ± 8.7	49.7 ± 6.4	−3.7%	52.6 ± 10.8	50.1 ± 8.9	−4.7%
HR-pQCT extended cortical measures						
Ct.vBMD	829 ± 68	805 ± 77	−3.0%	823 ± 53	818 ± 90	−0.6%
Ct.TMD	978 ± 39	968 ± 29	−1.1%	964 ± 30	970 ± 44	0.6%
Ct.Th	0.79 ± 0.19	0.79 ± 0.16	−0.7%	1.12 ± 0.23	1.19 ± 0.18	7.0%
Ct.PoV (mm^3)	9.11 ± 4.7	22.9 ± 32.6	**151.1%**[a]	55.8 ± 21.7	121 ± 213	117.5%
Ct.Po (%)	1.92 ± 0.90	4.29 ± 5.51	**123.9%**[a]	5.53 ± 2.00	7.53 ± 6.12	36.2%
ΔK_{PO} (%)	1.87 ± 0.91	2.97 ± 1.74	**58.8%**[a]	5.82 ± 2.45	6.66 ± 3.58	14.4%
ΔE_{PO} (%)	1.91 ± 0.92	3.00 ± 1.74	**56.9%**[a]	5.86 ± 2.45	6.70 ± 3.59	14.4%
ΔF_{PO} (%)	1.66 ± 0.93	2.52 ± 1.43	**51.8%**[a]	5.23 ± 2.50	5.80 ± 3.35	11.1%
ΔCt.LF$_{PO}$ (%)	1.77 ± 1.06	3.16 ± 2.45	**77.9%**[b]	5.62 ± 2.79	7.56 ± 6.16	34.5%

Data are expressed as mean ± SD. *Boldface* indicates statistically significant percentage difference: [a] $P < 0.05$; [b] $P < 0.01$.

in cortical microarchitecture of the T2DM cohort may be associated with a number of important covariates such as the age of onset of T2DM, disease severity, duration, and treatment. Furthermore, the two fracture subjects may represent a subset of the T2DM population that manifests significant architectural deterioration due to secondary causes associated with diabetes. Higher-powered epidemiological HR-pQCT studies are needed to address these questions more explicitly.

There are several limitations to this study to acknowledge. First, the limited number of subjects successfully recruited for this study (n = 38 total) precluded a direct examination and/or control for other potential covariates for the bone quality measures considered. This includes ethnicity, the age of onset of T2DM, the duration and severity of T2DM, treatment for T2DM, and the effect of other systemic complications related to diabetes. Furthermore, because only two of our T2DM patients had a history of fragility fracture, our results cannot directly address the question of fracture risk. It should be noted that although there were somewhat more African-American subjects in the T2DM group, vBMD, Ct.Th, and Tb.vBMD were not significantly different between African-American T2DM and the other pooled T2DM patients. Large cross-sectional case-control studies and prospective studies should be pursued to more rigorously investigate the relationship between bone quality measures and fracture risk in T2DM populations.

Additionally, the imaging sites were limited to 1-cm sections of the ultra distal end of the radius and tibia where a majority of the bone mass is cancellous, not cortical bone. This site was selected to be consistent with the manufacturer's default protocol, which has been applied in the vast majority of cross-sectional studies related to osteopenia and osteoporosis (22, 23, 29, 45). In the radius, bone strength estimates at this location have been shown to be well correlated to experimental mechanical behavior and approximately correspond spatially to the common Colles' fracture location (26). Although it is not possible to acquire mid-diaphyseal scans at the radius or tibia with this device, future studies could reliably include acquisitions up to 2 cm

more proximal where the relative bone mass is dominated by cortical bone (26, 62).

Finally, the standard trabecular bone analysis applied in this study employs several assumptions about bone matrix mineral density and marrow composition to calculate BV/TV which, in turn, is used to derive Tb.Th and Tb.Sp: namely, that both marrow composition and bone matrix mineral density are constant. Although variability in marrow composition is not likely a major source of error for peripheral skeletal sites, it is less clear how the degree of variability in bone matrix mineralization between these populations may be affected. In the cortex, our results indicate no significant difference in tissue level mineralization (Ct.TMD); however, this does not account for possible differences in microporosity not resolved by HR-pQCT. Furthermore, our analysis does not address the effect of matrix level differences in the organic phase of bone, which has been shown to be altered in association with T2DM (63).

In this study, we have characterized microarchitectural and biomechanical abnormalities in postmenopausal women with T2DM using noninvasive, high-resolution 3D imaging. The results of this pilot investigation provide a potential explanation for the inability of standard BMD measures to explain the elevated fracture incidence in patients with T2DM. Specifically, the findings suggest that T2DM may be associated with an inefficient redistribution of bone mass and insufficient compensation for increased body mass, which may result in impaired bending strength. These observations highlight the need for large, controlled, cross-sectional and longitudinal studies of bone quality in T2DM cohorts as well as prospective studies of fracture risk in this population. Collectively, this study has used HR-pQCT to identify microarchitectural deficits in the cortical bone of patients with T2DM compared with normal CTRLs.

Acknowledgments

The authors thank Thelma Munoz, Jingyi Yu, Nicole Cheng, Melissa Guan, and Ayako Suzuki for contributions in recruiting subjects, image acquisition, and database management. The authors additionally thank Dr. Andres Laib and Scanco Medical AG for providing software development documentation and resources and for countless helpful technical discussions.

Address all correspondence and requests for reprints to: Andrew J. Burghardt, Musculoskeletal Quantitative Imaging Research Group, Department of Radiology and Biomedical Imaging, University of California, San Francisco, QB3 Building, Suite 203, 1700 4th Street, San Francisco, California 94158. E-mail: andrew.burghardt@ucsf.edu.

This work was supported by National Institutes of Health (NIH)/National Center for Research Resources (NCRR), University of California, San Francisco (UCSF)-Clinical and Translational Science Institute Grant UL1 RR024131-01 (to A.J.B.), NIH Grant R01 AG17762 (to S.M.), NIH Grant RC1 AR058405-01 (to T.M.L.), and a UCSF Research Evaluation and Allocation Committee Grant (to T.M.L.).

Disclosure Summary: The authors have no financial disclosures or conflicts of interest.

References

1. **Janghorbani M, Van Dam RM, Willett WC, Hu FB** 2007 Systematic review of type 1 and type 2 diabetes mellitus and risk of fracture. Am J Epidemiol 166:495–505
2. **Yamamoto M, Yamaguchi T, Yamauchi M, Kaji H, Sugimoto T** 2009 Diabetic patients have an increased risk of vertebral fractures independent of BMD or diabetic complications. J Bone Miner Res 24:702–709
3. **Forsén L, Meyer HE, Midthjell K, Edna TH** 1999 Diabetes mellitus and the incidence of hip fracture: results from the Nord-Trondelag Health Survey. Diabetologia 42:920–925
4. **Ottenbacher KJ, Ostir GV, Peek MK, Goodwin JS, Markides KS** 2002 Diabetes mellitus as a risk factor for hip fracture in Mexican American older adults. J Gerontol A Biol Sci Med Sci 57:M648–M653
5. **Nicodemus KK, Folsom AR** 2001 Type 1 and type 2 diabetes and incident hip fractures in postmenopausal women. Diabetes Care 24:1192–1197
6. **Schwartz AV, Sellmeyer DE, Ensrud KE, Cauley JA, Tabor HK, Schreiner PJ, Jamal SA, Black DM, Cummings SR** 2001 Older women with diabetes have an increased risk of fracture: a prospective study. J Clin Endocrinol Metab 86:32–38
7. **Chu SP, Kelsey JL, Keegan TH, Sternfeld B, Prill M, Quesenberry CP, Sidney S** 2004 Risk factors for proximal humerus fracture. Am J Epidemiol 160:360–367
8. **Keegan TH, Kelsey JL, Sidney S, Quesenberry Jr CP** 2002 Foot problems as risk factors of fractures. Am J Epidemiol 155:926–931
9. **Leidig-Bruckner G, Ziegler R** 2001 Diabetes mellitus a risk for osteoporosis? Exp Clin Endocrinol Diabetes 109 Suppl 2:S493–S514
10. **Buysschaert M, Cauwe F, Jamart J, Brichant C, De Coster P, Magnan A, Donckier J** 1992 Proximal femur density in type 1 and 2 diabetic patients. Diabete Metab 18:32–37
11. **Hampson G, Evans C, Petitt RJ, Evans WD, Woodhead SJ, Peters JR, Ralston SH** 1998 Bone mineral density, collagen type 1 α 1 genotypes and bone turnover in premenopausal women with diabetes mellitus. Diabetologia 41:1314–1320
12. **Tuominen JT, Impivaara O, Puukka P, Rönnemaa T** 1999 Bone mineral density in patients with type 1 and type 2 diabetes. Diabetes Care 22:1196–1200
13. **Vestergaard P** 2007 Discrepancies in bone mineral density and fracture risk in patients with type 1 and type 2 diabetes—a meta-analysis. Osteoporos Int 18:427–444
14. **Melton 3rd LJ, Riggs BL, Leibson CL, Achenbach SJ, Camp JJ, Bouxsein ML, Atkinson EJ, Robb RA, Khosla S** 2008 A bone structural basis for fracture risk in diabetes. J Clin Endocrinol Metab 93:4804–4809
15. **Orwoll ES, Bauer DC, Vogt TM, Fox KM** 1996 Axial bone mass in older women. Study of Osteoporotic Fractures Research Group. Ann Intern Med 124:187–196
16. **van Daele PL, Stolk RP, Burger H, Algra D, Grobbee DE, Hofman A, Birkenhäger JC, Pols HA** 1995 Bone density in non-insulin-dependent diabetes mellitus. The Rotterdam Study. Ann Intern Med 122:409–414
17. **Barrett-Connor E, Kritz-Silverstein D** 1996 Does hyperinsulinemia preserve bone? Diabetes Care 19:1388–1392
18. **Bauer DC, Browner WS, Cauley JA, Orwoll ES, Scott JC, Black DM,**

Tao JL, Cummings SR 1993 Factors associated with appendicular bone mass in older women. The Study of Osteoporotic Fractures Research Group. Ann Intern Med 118:657–665

19. **MacNeil JA, Boyd SK** 2007 Accuracy of high-resolution peripheral quantitative computed tomography for measurement of bone quality. Med Eng Phys 29:1096–1105
20. **Burghardt AJ, Kazakia GJ, Majumdar S** 2007 A local adaptive threshold strategy for high resolution peripheral quantitative computed tomography of trabecular bone. Ann Biomed Eng 35:1678–1686
21. **Liu XS, Zhang XH, Sekhon KK, Adams MF, McMahon DJ, Bilezikian JP, Shane E, Guo XE** 2010 High-resolution peripheral quantitative computed tomography can assess microstructural and mechanical properties of human distal tibial bone. J Bone Miner Res 25:746–756
22. **Boutroy S, Bouxsein ML, Munoz F, Delmas PD** 2005 *In vivo* assessment of trabecular bone microarchitecture by high-resolution peripheral quantitative computed tomography. J Clin Endocrinol Metab 90:6508–6515
23. **Khosla S, Riggs BL, Atkinson EJ, Oberg AL, McDaniel LJ, Holets M, Peterson JM, Melton 3rd LJ** 2006 Effects of sex and age on bone microstructure at the ultradistal radius: a population-based noninvasive in vivo assessment. J Bone Miner Res 21:124–131
24. **Kirmani S, Christen D, van Lenthe GH, Fischer PR, Bouxsein ML, McCready LK, Melton 3rd LJ, Riggs BL, Amin S, Müller R, Khosla S** 2009 Bone structure at the distal radius during adolescent growth. J Bone Miner Res 24:1033–1042
25. **Dalzell N, Kaptoge S, Morris N, Berthier A, Koller B, Braak L, van Rietbergen B, Reeve J** 2009 Bone micro-architecture and determinants of strength in the radius and tibia: age-related changes in a population-based study of normal adults measured with high-resolution pQCT. Osteoporos Int 20:1683–1694
26. **Mueller TL, van Lenthe GH, Stauber M, Gratzke C, Eckstein F, Müller R** 2009 Regional, age and gender differences in architectural measures of bone quality and their correlation to bone mechanical competence in the human radius of an elderly population. Bone 45:882–891
27. **Burrows M, Liu D, McKay H** 2010 High-resolution peripheral QCT imaging of bone micro-structure in adolescents. Osteoporos Int 21:515–520
28. **Melton 3rd LJ, Riggs BL, van Lenthe GH, Achenbach SJ, Müller R, Bouxsein ML, Amin S, Atkinson EJ, Khosla S** 2007 Contribution of in vivo structural measurements and load/strength ratios to the determination of forearm fracture risk in postmenopausal women. J Bone Miner Res 22:1442–1448
29. **Sornay-Rendu E, Boutroy S, Munoz F, Delmas PD** 2007 Alterations of cortical and trabecular architecture are associated with fractures in postmenopausal women, partially independent of decreased BMD measured by DXA: the OFELY study. J Bone Miner Res 22:425–433
30. **Boutroy S, Van Rietbergen B, Sornay-Rendu E, Munoz F, Bouxsein ML, Delmas PD** 2008 Finite element analysis based on in vivo HR-pQCT images of the distal radius is associated with wrist fracture in postmenopausal women. J Bone Miner Res 23:392–399
31. **Vico L, Zouch M, Amirouche A, Frère D, Laroche N, Koller B, Laib A, Thomas T, Alexandre C** 2008 High-resolution pQCT analysis at the distal radius and tibia discriminates patients with recent wrist and femoral neck fractures. J Bone Miner Res 23:1741–1750
32. **Chavassieux P, Asser Karsdal M, Segovia-Silvestre T, Neutzsky-Wulff AV, Chapurlat R, Boivin G, Delmas PD** 2008 Mechanisms of the anabolic effects of teriparatide on bone: insight from the treatment of a patient with pycnodysostosis. J Bone Miner Res 23:1076–1083
33. **Bacchetta J, Boutroy S, Vilayphiou N, Juillard L, Guebre-Egziabher F, Rognant N, Sornay-Rendu E, Szulc P, Laville M, Delmas PD, Fouque D, Chapurlat R** 2010 Early impairment of trabecular microarchitecture assessed with HR-pQCT in patients with stage II–IV chronic kidney disease. J Bone Miner Res 25:849–857
34. **Rubin MR, Dempster DW, Kohler T, Stauber M, Zhou H, Shane E, Nickolas T, Stein E, Sliney Jr J, Silverberg SJ, Bilezikian JP, Müller R** 2010 Three dimensional cancellous bone structure in hypoparathyroidism. Bone 46:190–195
35. **Schwartz AV, Sellmeyer DE** 2007 Diabetes, fracture, and bone fragility. Curr Osteoporos Rep 5:105–111
36. **Burghardt AJ, Kazakia GJ, Ramachandran S, Link TM, Majumdar S** 2010 Age- and gender-related differences in the geometric properties and biomechanical significance of intracortical porosity in the distal radius and tibia. J Bone Miner Res 25:983–993
37. **Feldkamp LA, Davis LC, Kress JW** 1984 Practical cone-beam algorithm. J Opt Soc Am A 1:612–619
38. **Burghardt AJ, Kazakia GJ, Laib A, Majumdar S** 2008 Quantitative assessment of bone tissue mineralization with polychromatic micro-computed tomography. Calcif Tissue Int 83:129–138
39. **Laib A, Häuselmann HJ, Rüegsegger P** 1998 In vivo high resolution 3D-QCT of the human forearm. Technol Health Care 6:329–337
40. **Laib A, Rüegsegger P** 1999 Calibration of trabecular bone structure measurements of in vivo three-dimensional peripheral quantitative computed tomography with 28-microm-resolution microcomputed tomography. Bone 24:35–39
41. **Burghardt AJ, Kazakia GJ, Link TM, Majumdar S** 2009 Automated simulation of areal bone mineral density assessment in the distal radius from high-resolution peripheral quantitative computed tomography. Osteoporos Int 20:2017–2024
42. **Laib A, Rüegsegger P** 1999 Comparison of structure extraction methods for in vivo trabecular bone measurements. Comput Med Imaging Graph 23:69–74
43. **Hildebrand T, Ruegsegger P** 1997 A new method for the model-independent assessment of thickness in three-dimensional images. J Microsc 185:67–75
44. **Laib A, Hildebrand T, Häuselmann HJ, Rüegsegger P** 1997 Ridge number density: a new parameter for in vivo bone structure analysis. Bone 21:541–546
45. **Kazakia GJ, Hyun B, Burghardt AJ, Krug R, Newitt DC, de Papp AE, Link TM, Majumdar S** 2008 In vivo determination of bone structure in postmenopausal women: a comparison of HR-pQCT and high-field MR imaging. J Bone Miner Res 23:463–474
46. **MacNeil JA, Boyd SK** 2008 Improved reproducibility of high-resolution peripheral quantitative computed tomography for measurement of bone quality. Med Eng Phys 30:792–799
47. **Mueller TL, Stauber M, Kohler T, Eckstein F, Müller R, van Lenthe GH** 2009 Non-invasive bone competence analysis by high-resolution pQCT: an in vitro reproducibility study on structural and mechanical properties at the human radius. Bone 44:364–371
48. **Buie HR, Campbell GM, Klinck RJ, MacNeil JA, Boyd SK** 2007 Automatic segmentation of cortical and trabecular compartments based on a dual threshold technique for in vivo micro-CT bone analysis. Bone 41:505–515
49. **Nishiyama KK, Macdonald HM, Buie HR, Hanley DA, Boyd SK** 2010 Postmenopausal women with osteopenia have higher cortical porosity and thinner cortices at the distal radius and tibia than women with normal aBMD: an in vivo HR-pQCT study. J Bone Miner Res 25:882–890
50. **Burghardt AJ, Buie HR, Laib A, Majumdar S, Boyd SK** 1 June 2010 Reproducibility of direct quantitative measures of cortical bone microarchitecture of the distal radius and tibia by HR-pQCT. Bone doi:10.1016/j.bone.2010.05.034
51. **Müller R, Rüegsegger P** 1995 Three-dimensional finite element modelling of non-invasively assessed trabecular bone structures. Med Eng Phys 17:126–133
52. **van Rietbergen B, Weinans H, Huiskes R, Odgaard A** 1995 A new method to determine trabecular bone elastic properties and loading using micromechanical finite-element models. J Biomech 28:69–81
53. **Van Rietbergen B, Odgaard A, Kabel J, Huiskes R** 1996 Direct

mechanics assessment of elastic symmetries and properties of trabecular bone architecture. J Biomech 29:1653–1657
54. **Pistoia W, van Rietbergen B, Lochmüller EM, Lill CA, Eckstein F, Rüegsegger P** 2002 Estimation of distal radius failure load with micro-finite element analysis models based on three-dimensional peripheral quantitative computed tomography images. Bone 30:842–848
55. **Genant HK, Wu CY, van Kuijk C, Nevitt MC** 1993 Vertebral fracture assessment using a semiquantitative technique. J Bone Miner Res 8:1137–1148
56. **Petit MA, Paudel ML, Taylor BC, Hughes JM, Strotmeyer ES, Schwartz AV, Cauley JA, Zmuda JM, Hoffman AR, Ensrud KE** 2010 Bone mass and strength in older men with type 2 diabetes: the Osteoporotic Fractures in Men Study. J Bone Miner Res 25:285–291
57. **Yeni YN, Brown CU, Wang Z, Norman TL** 1997 The influence of bone morphology on fracture toughness of the human femur and tibia. Bone 21:453–459
58. **Voide R, Schneider P, Stauber M, Wyss P, Stampanoni M, Sennhauser U, van Lenthe GH, Müller R** 2009 Time-lapsed assessment of microcrack initiation and propagation in murine cortical bone at submicrometer resolution. Bone 45:164–173
59. **Zhang L, Liu Y, Wang D, Zhao X, Qiu Z, Ji H, Rong H** 2009 Bone biomechanical and histomorphometrical investment in type 2 diabetic Goto-Kakizaki rats. Acta Diabetol 46:119–126
60. **Prisby RD, Swift JM, Bloomfield SA, Hogan HA, Delp MD** 2008 Altered bone mass, geometry and mechanical properties during the development and progression of type 2 diabetes in the Zucker diabetic fatty rat. J Endocrinol 199:379–388
61. **Kawashima Y, Fritton JC, Yakar S, Epstein S, Schaffler MB, Jepsen KJ, LeRoith D** 2009 Type 2 diabetic mice demonstrate slender long bones with increased fragility secondary to increased osteoclastogenesis. Bone 44:648–655
62. **Boyd SK** 2008 Site-specific variation of bone micro-architecture in the distal radius and tibia. J Clin Densitom 11:424–430
63. **Paul RG, Bailey AJ** 1996 Glycation of collagen: the basis of its central role in the late complications of ageing and diabetes. Int J Biochem Cell Biol 28:1297–1310